The 14th International Topical Meeting on Nuclear Reactor Thermalhydraulics, NURETH-14
Toronto, Ontario, Canada, September 25-30, 2011

NURETH14-221

CHEMICAL EFFECTS AND THE IMPACT TO INSULATION DEBRIS FILTER CAKES AT ECCS UPSTREAM AND DOWNSTRAM COMPONENTS

S. Alt[1], M. Hölker[1], W. Hoffmann[2], W. Kästner[1], H. Kryk[2], S. Renger[1] and A. Seeliger[1]
[1] University of Applied Sciences Zittau/Goerlitz, Germany
[2] Helmholtz-Zentrum Dresden-Rossendorf

Abstract

Investigations regarding release, solution, transportation and deposit of corrosion products become important to reactor safety research for PWR, when considering the long-term behaviour of emergency core cooling systems (ECCS) during loss of coolant accidents (LOCA). The knowledge of corrosion processes in boric acid is necessary to evaluate the impact on insulation debris filter cakes in upstream (sump strainers) and downstream (reactor core) components and their influence on head loss and heat removal out of the core. Generic complex experiments determined the quantity of flow-induced, released corrosion products and their influences on head losses at filter cakes.

Introduction

The investigations regarding release, solubility, transportation and deposit of corrosion products become important to reactor safety research for PWR and BWR, when considering the long-term behaviour of emergency core cooling systems during loss of coolant accidents (LOCA). The knowledge of these processes is necessary to evaluate the impact on insulation debris filter cakes in upstream (sump strainers) and downstream (reactor core) components and their influence on head loss and heat removal out of the core [1]. The design of complex experiments was focused to the impact of corrosion processes at hot-dip galvanized steel gratings in water and boric acid. Additional substances were not considered in these experiments. This paper includes the description of the experimental facility for the complex generic experiments, an overview of experimental boundary conditions, the dependence between solubility, corrosion rate and their impact on head losses as results of corrosion experiments. A well mixing of air in the fluid was also considered by free jet expansions and flows through full cone-nozzles above the sump level. The influences of coupled effects during the long-term behaviour were investigated in a large scaled sump model "Zittauer Strömungswanne (ZSW)" that was connected with a single shortened FA-dummy with 3 spacers and a debris filter at the FA-bottom.

1. Motivation and objectives of the investigations

Figure 1 shows an overview about the scenario and the hydro-dynamic processes during a postulated LOCA with a release of fragmented insulation material. Flow parameters were determined on the basis of separate and complex experiments [3-5] and CFD-modelling and -simulations were realized [6-7] for the short-term behaviour of the different processes. The long-term behaviour of these processes is additionally influenced by corrosion processes at hot-dip galvanized steel gratings, which are located in the containment. The following phenomena have to be considered for modelling:

- production of soluble ions and particulate corrosion products at hot-dip galvanized gratings,
- their influence on the cooling water chemistry and vice versa,
- transportation of latent corrosion products from the gratings to the sump strainers,
- deposition of corrosion particles at insulation fibre beds as well as
- their influence on head loss at sump strainers and/or in the reactor core.

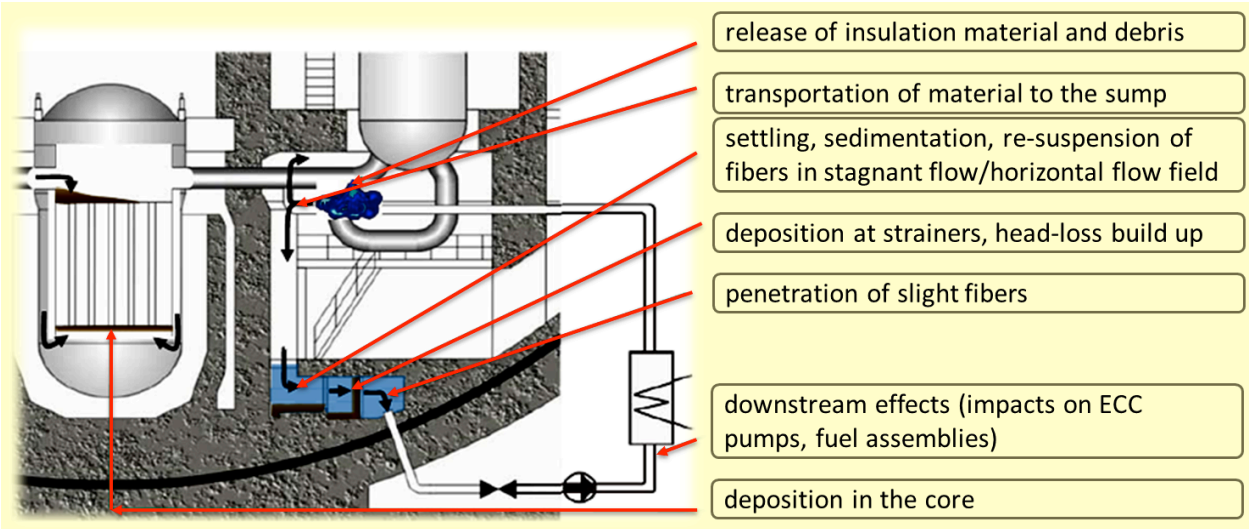

Figure 1: Schematic of a postulated LOCA scenario in PWR.

Separate effect and generic complex experiments were performed to determine the quantity of released corrosion products that can form in LOCA specific sump environment of NPP. The initial water chemistry during the experiments was characterized by deionized water conditions in sumps and wet-wells of BWR and an addition of app. 2300…2500 ppm boric acid (13 g/l H_3BO_3) in sumps of PWR for generic assumed conditions. This paper focuses on the experiments with boric acid and shows the further knowledge development in comparison to [8-9].

2. Description of the sump model "Zittauer Strömungswanne (ZSW)"

The geometry and dimensions of a simplified sump model were scaled on the basis of a generic PWR according to German PWR conditions. Upstream generic PWR sump data in front of the sump strainer were selected on the following basis:

- original dimension of the generic reactor sump height up to 3.0 m,
- original flow path length for the duration of the transport of mineral wool from the break location to the sump strainer up to 5.5 m,
- simplified rectangular flow cross section in the upstream region without obstacles,
- volume dependent scaling of sump strainer surface area, pump volume flow,
- stable materials (stainless steel, acrylic glass ➔ temperatures up to 70°C, chemical resistance).

The construction and geometric conditions of the ZSW are illustrated in Figure 2. The P&I diagram of the facility with a single shortened PWR-fuel assembly (FA)-dummy is shown in Figure 3. According to two LOCA-scenarios (leakage in hot leg, leakage in cold leg) and the positions of ECC-injections in the hot and in the cold loops of the primary system in German PWR the FA-dummy can be passed by the emergency coolant in upward as well as in downward flow direction [2].

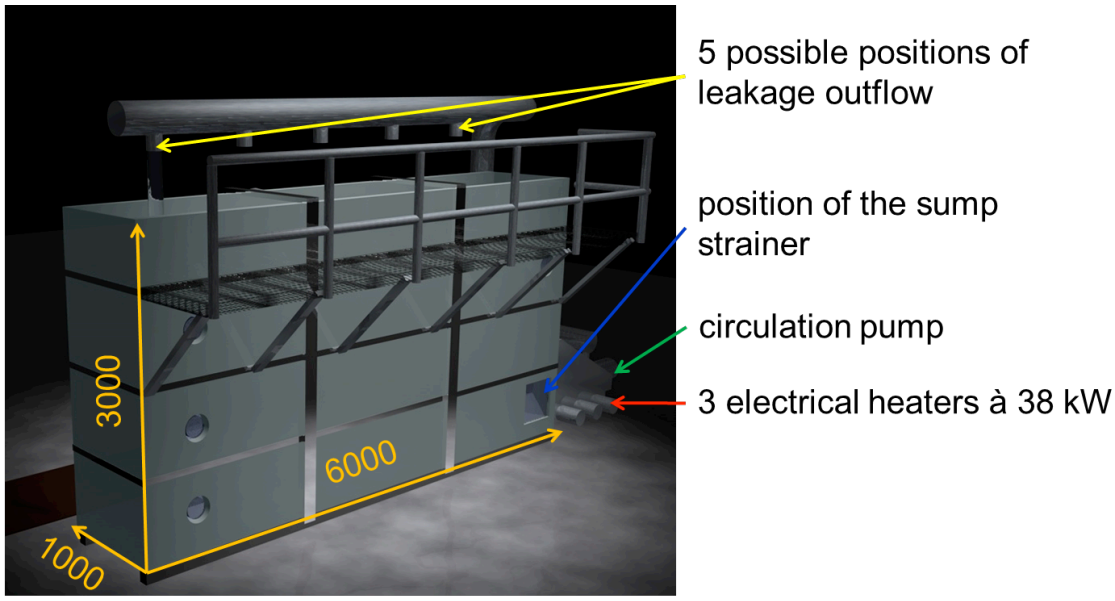

Figure 2: Sump model dimensions of the "ZSW" facility.

The single shortened PWR-FA-dummy consists of

- 16 x 16 fuel rod dummies, 20 control rod simulators, three spacers,
- FA-head and FA-bottom with integrated debris-filter screen (IDF).

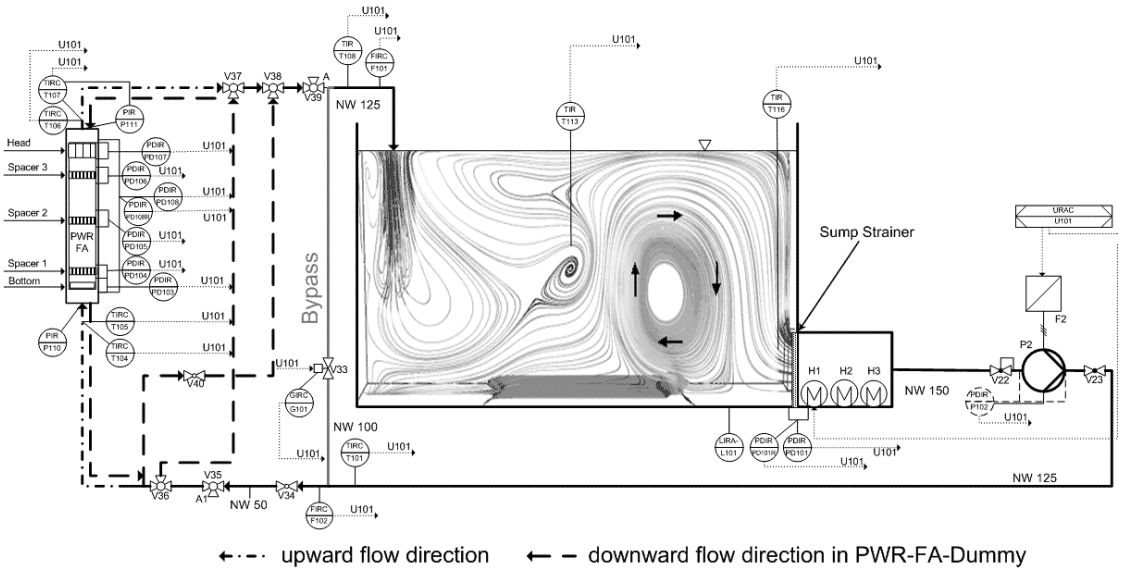

Figure 3: P&I diagram of "ZSW"-facility with a single shortened PWR-FA-Dummy.

The FA-dummy is encased with an acrylic glass housing. The experiments involved measuring and recording of differential pressures (head losses) across the FA-bottom, the three spacers, the FA-head and the FA as a whole. The configuration of the FA-dummy test section and head loss-instrumentation is shown in Figure 4.

Figure 4: FA-dummy test-section with head loss-instrumentation.

3. Boundary conditions of ZSW-corrosion experiments

The timetable of the long-term corrosion experiments at ZSW with single FA-dummy was divided into the following phases:

- preparation of insulation material (artificial aging, steam fragmentation),
- sump fill-up and injection of insulation-water-suspensions without recirculation,
- pump start, recirculation (short-term phenomena) and
- long-term operation.

The fill-up procedure and the short-term upstream and downstream experimental results (distribution of sediments at the sump bottom, agglomeration mass at the sump strainer, penetration to the downstream FA-dummy, head losses at the strainer and in the FA-dummy) are described in detail in [9]. The main geometric and fluid-dynamic boundary conditions were constant for four experiments (V12, V18, V16J, V18J) to compare the influences of different corrosion surfaces on the long-term results:

- sump strainer (3 mm x 3 mm vertical flat screen): 0.42 m²
- superficial sump strainer velocity: 2.9 cm/s
- fluid temperature: 45 °C
- boric acid concentration: 13 g/l
- dry mass of released insulation material: 985 g MD2 (mineral wool)
- flow direction in the FA-dummy: upwards

The hot-dip galvanizing manufacturing method was used for the production of all zinc coatings at the steel gratings. These hot-dip galvanized steel gratings (GR) were installed in the upwards region in front of the sump strainer as corrodible material with respect to different flow conditions:

- immersed under the sump level without impact from the leakage spray jet (Figure 5)
- mounted above the sump level under the leakage spray jet (Figure 6)
- both configurations simultaneously (Figure 6).

The data of the installed hot-dip galvanized steel gratings are shown in Table 1. The difference between the experiments consisted in the number of plunged zinc coated gratings, the corrodible mass and surface, respectively. The gratings were completely plunged under the coolant surface during the experiments V12 and V18. The total corrodible surface area and the mass of the gratings were reduced

for experiment V18 by a ratio of 1:3 in comparison to V12. The experiment V16J was carried out with a single grating under the leakage spray jet and in V18J a combination of both installations was considered.

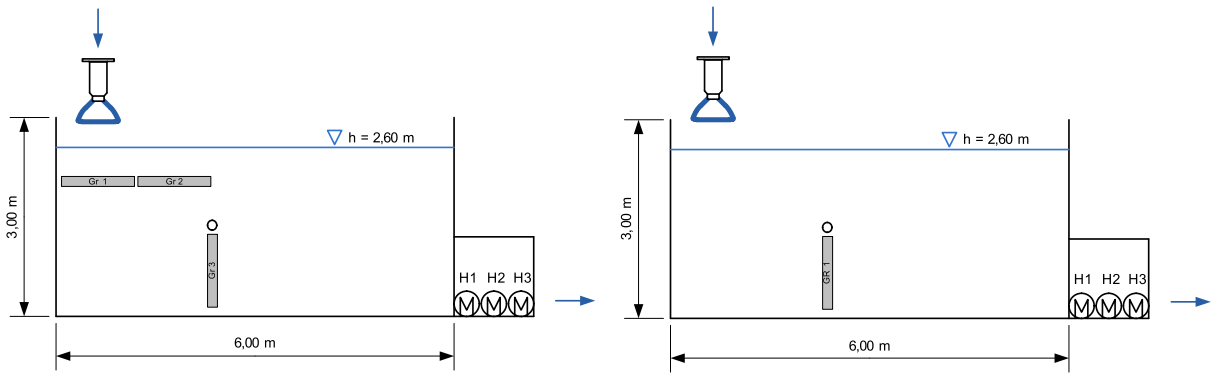

Figure 5: Positions of immersed gratings for experiments V12 (left) and V18 (right).

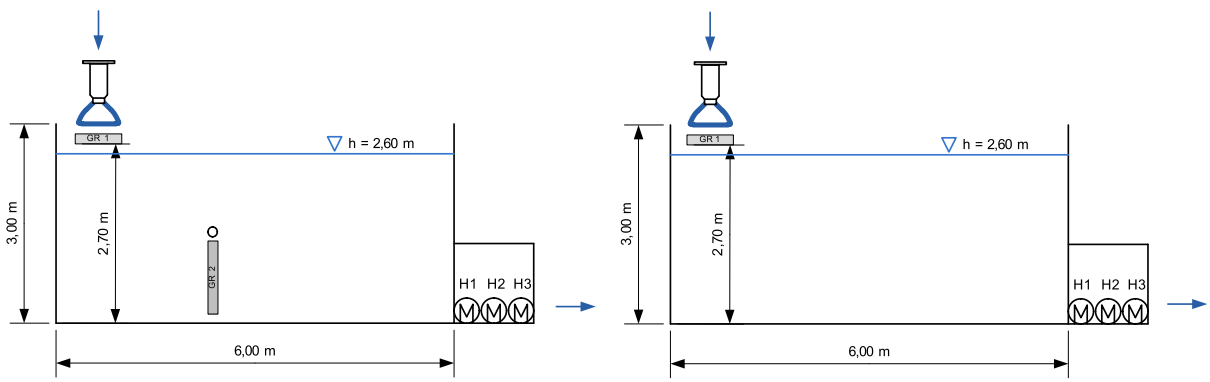

Figure 6: Positions of gratings for experiments V18J (left) and V16J (right).

Condition	V12	V18	V16J	V18J
Hot-dip galvanized steel gratings (GR)	3 units (immersed) (1006x990x4) 77.715 kg	1 unit (immersed) (1006x990x4) 25.940 kg	1 unit (jet) (450x450x4) 5.568 kg	1 unit (jet) (450x450x4) 5.585 kg 1 unit immersed (1006x990x4) 25.910 kg
Corrosion surface (CS)	≈ 9.33 m² (immersed)	≈ 3.11 m² (immersed)	≈ 0.69 m² (jet)	≈ 0.69 m² (jet) ≈ 3.11 m² (immersed)
CS/Fluid Volume	0.6 m²/m³	0.2 m²/m³	0.044 m²/m³	0.044 m²/m³ 0.2 m²/m³

Table 1: Boundary conditions for long-term corrosion experiments at ZSW

4. Long-term experimental results and chemical phenomena

4.1 Upstream Results

Figure 7 shows the post-test sediment distributions at the bottom of the ZSW sump model of the four experiments. The largest amount of sediments directly appeared at the ground floor under the leakage spray that also was the location of fibre-suspension-injections. The sediment distribution decreased towards the sump strainer and indicates the existence of internal vortices in the sump volume. The filter cakes of the sump strainer were fallen down after shutdown and outflow of the fluid or were caused by back-flushing procedures.

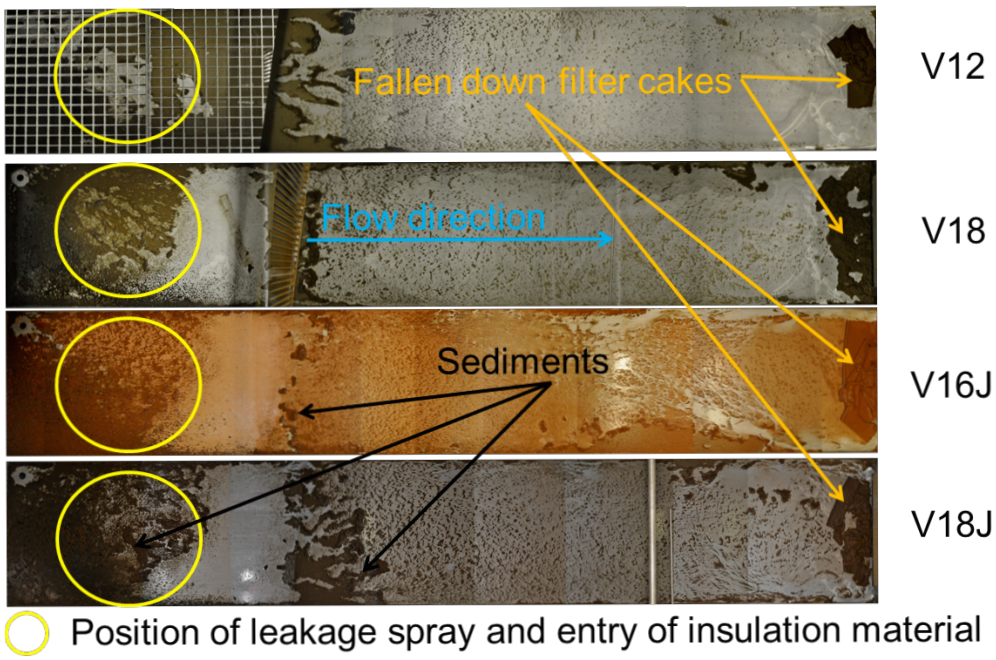

Figure 7: Sediment distributions at the bottom of the ZSW sump model.

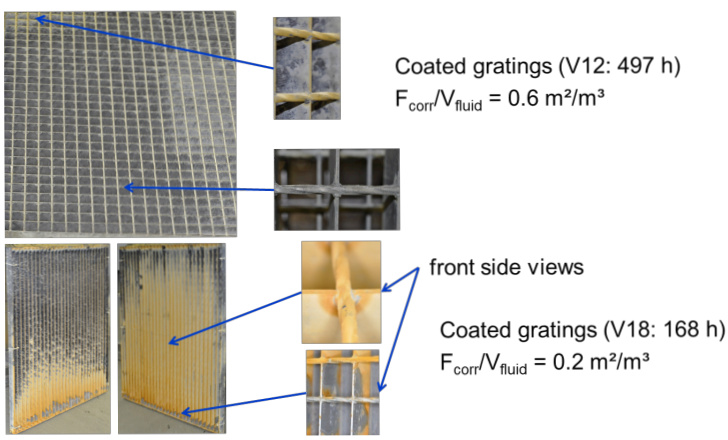

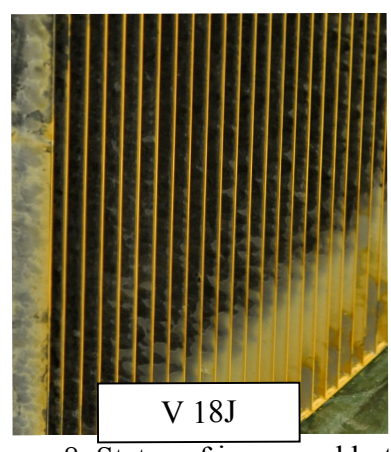

Figure 8: Status of immersed hot-dip galvanized steel gratings.

The three immersed gratings of experiment V12 mainly showed a grey rough surface with minimal local brown colorations after the experimental run (upper photos in Figure 8, left side). The immersed grating of experiment V18 showed larger amounts of rust-brown released materials at the surface contrary to V12. The constitution of the immersed gratings does not essentially differ between the experiments V18 and V18J. The impacts of jet leakage sprays on hot-dip galvanized surfaces (V16J and V18J) installed over the sump level showed other situations of the grating´s surfaces. The zinc-layers

were completely removed from the gratings and the corrosion progressed through the pure steel (Figure 9).

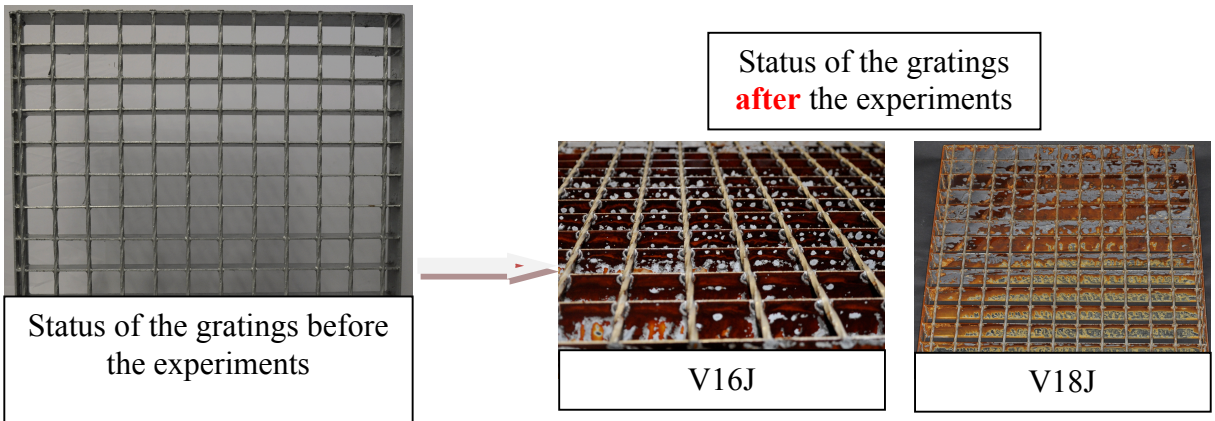

f the zinc-layer and rustingt the jet steel gratings in V16 and V18J.

on products and their composition (zinc-ions, rust particles) influenced
p at the sump strainers. The gradients of the long-term head losses are

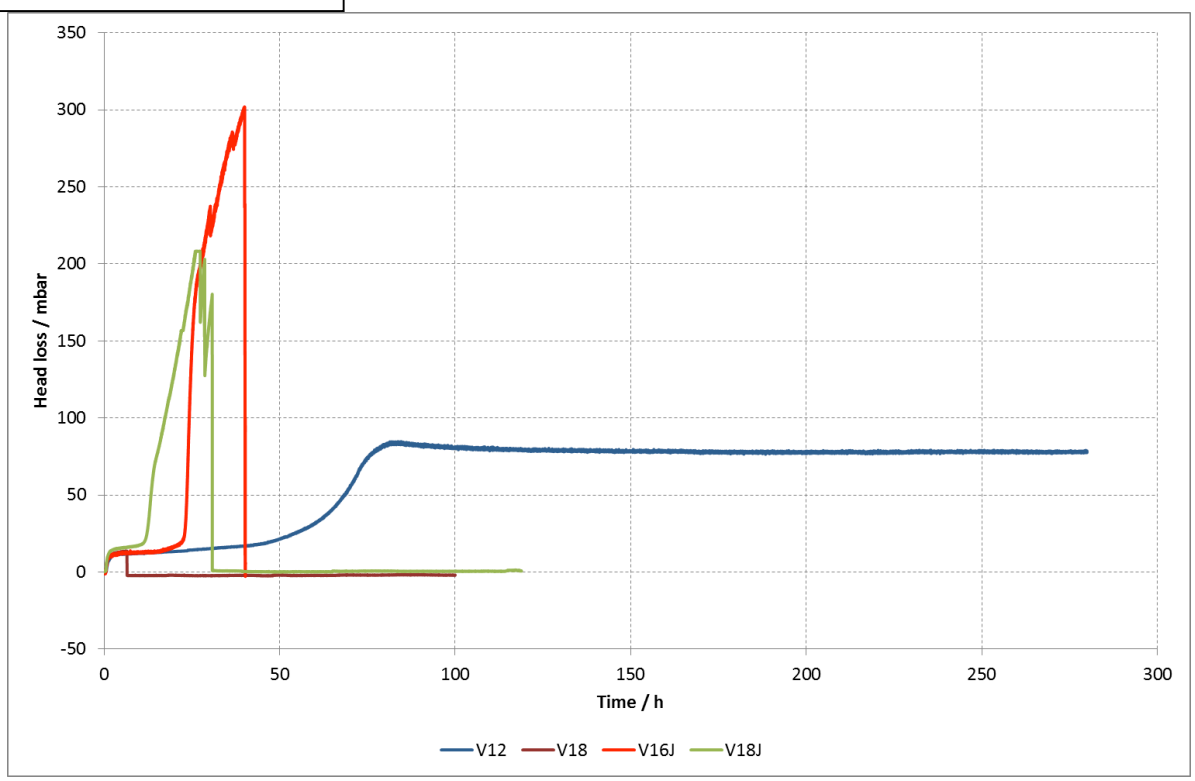

Figure 10: Long-term head loss build up at the sump strainer.

The behaviour of the gradients was caused by experimental conditions and can be described as follows.
V12:

- quasi steady-state head loss (short-term) up to 45 h, significant increase of head loss after 45 h
- damping of head loss increase after 80 hours, stabilization at 80 mbar for long period (200 h)

V18:

- quasi steady-state head loss (short-term)
- electrical blackout with pump shut down after 6 h 32 min, 6 h 35 min: restart of pump, no further re-covering of the sump strainer, no head loss at the strainer
- passing of corrosion products to downstream FA-dummy

V16J, V18J:

- quasi steady-state head loss (short-term)
- rapid increase of head loss after 12 h up to 200 mbar (V18J)
- rapid increase of head loss after 22 h up to 300 mbar (V16J)
- stepwise reduction of volume flow rate down to stagnant flow
- back-flushing of the sump strainer, restart of recirculation without re-covering of the sump strainer, passing of corrosion products to downstream FA-dummy

4.2 Downstream Results

When the time of fibre penetration at the sump strainers was long enough (before complete formation of the sump strainer filter cakes) the fibres were transported to the downstream FA-dummy and mainly agglomerated at the IDF (for upstream flow) or the 3rd Spacer (for downstream flow). Figure 11 exemplarily shows a filter cake at the IDF after a long-term experiment with back-flushing of the sump strainer filter cake. The corrosion products were passed through the free sump strainer caused by the unavailable filter effect and flowed to the FA filter cakes. The results of the EDX-analyses show the brown coloured filter cakes mainly included iron (rust particles). Zinc fractions were enclosed in the filter bed with a ratio of about 1/10 to iron. The rust particles agglomerated onto the fibres in the filter cakes in comparison to short-term experiments without corrosion processes (Figure 12). The increase of friction loss and the decrease of the filter cake porosity were the reasons for the increased head losses at the sump strainer (Figure 10) and after back-flushing in the FA-dummy (Figure 13). However, the time-dependent head loss build up is a consequence of the release rate of corrosion products caused by chemistry (particularly of the time-dependent process, when rust particle released out of the hard alloy layer or the pure steel), the momentum of the flow impact on the gratings (immersed, under forced spray), the ratio of corrosion surface/fluid volume.

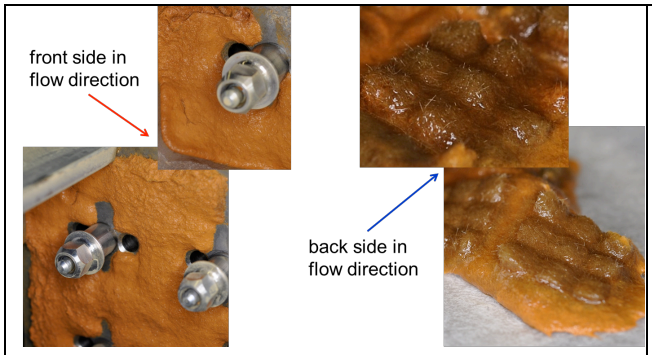

Figure 11: Fiber disposals at the IDF of the FA-bottom with impact of corrosion products

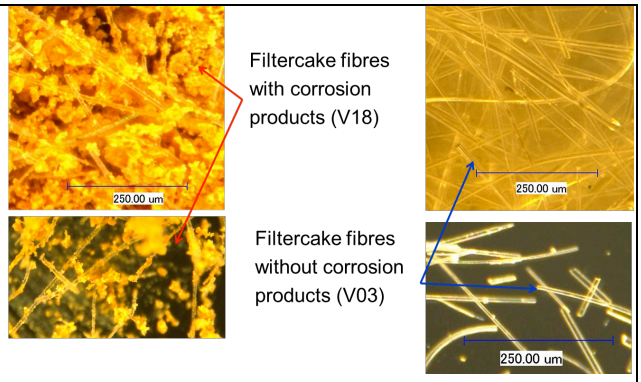

Figure 12: Microscopic view of the corrosion products adhesion in fibre beds

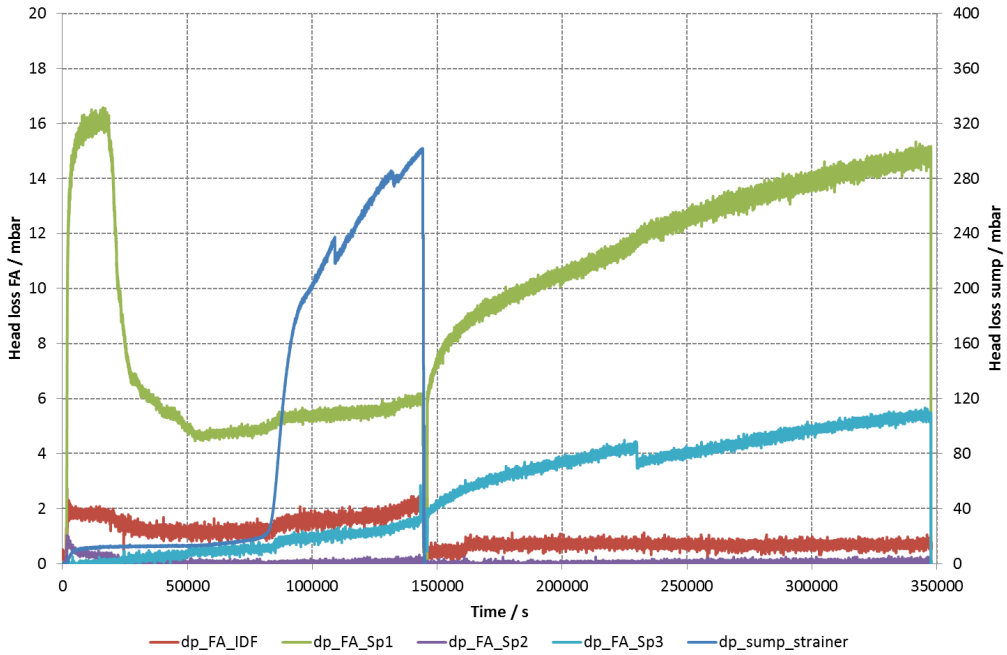

Figure 13: Long-term head loss build up in the FA-dummy after back-flushing at the sump strainer.

4.3 Corrosion mechanism at hot-dip galvanized steel gratings and chemistry in boric acid fluids

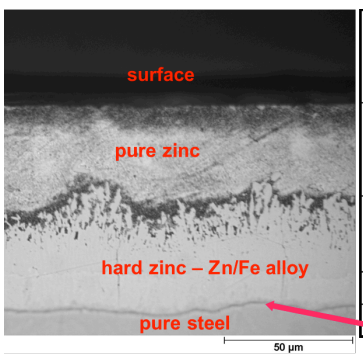

layer	m_{Zn} %	m_{Fe} %	nano hardness GPa
η	100	-	0,9
ζ	94	6	2,6
δ	90	10	3,9
γ	75	25	

Nano hardness of steel: 2,6 GPa

The behaviour of flow-induced corrosion processes on surfaces depends on the composition and structure of the corroding material. The structure of hot-dip galvanized steel gratings is characterized by an increase in iron content in the different layers from the surface up to the pure steel base material shown in Figure 14.

.

Figure 14: Cross section and properties of hot-dip galvanized steel gratings.

The corrosion process begins at the surface of hot-dip galvanized steel gratings under the impact of flowing boric acid. The upper layer (η-layer) consists of pure (supple) zinc. Soluble zinc-borat-ions will be produced and cause an increase of Zn^{2+} und OH^- ions. A lower pH-value forced the corrosion process. Higher Zn^{2+} concentrations in the fluid decelerate the zinc corrosion process. Solid corrosion particles will not appear in the fluid if the progress of the corrosion process does not spread throughout the η-layer. The corrosion process additionally influences the chemical consistence of the fluid. The equilibrium potential of chemical compounds of zinc corrosion products (Zn^{2+}, ZnO, Zn-carbonate and zinc-borat) in boric acid depends on the concentration of boric acid in water, fluid temperature, pH-value, free fluid surfaces in contact with air (dioxygen, carbon dioxide), contact area with corrosion materials. The generation of ZnO and alkaline Zn-carbonate will be effected at neutral pH-values. The lowest concentrated compound will be deposited out of the equilibrium. Loss of ions out of the equilibrium will be compensated through dissociation. The

potential of Zn/Fe-alloy increases with rising iron-concentration. This increased potential causes a preferred dissolving of Zn-abounded alloy. Iron-ions will be dissolved during the corrosion of the alloy-layer (Figure 14) at low pH-values. Rust will be produced at higher pH-values. A jet impact or flow field is necessary for the discharge of corrosion products (ions and rust particles) from the corrosion surface into the fluid and later for the agglomeration in the fiber beds of insulation material at the sump strainers.

4.4 Experimental release behaviour of corrosion products

The gradients of conductivity, pH-value and zinc-ion-concentration in the boric acid are shown in Figure 15. Rising pH-values based on increased zinc-concentrations and the relation between conductivity and zinc-concentration directly correlates.

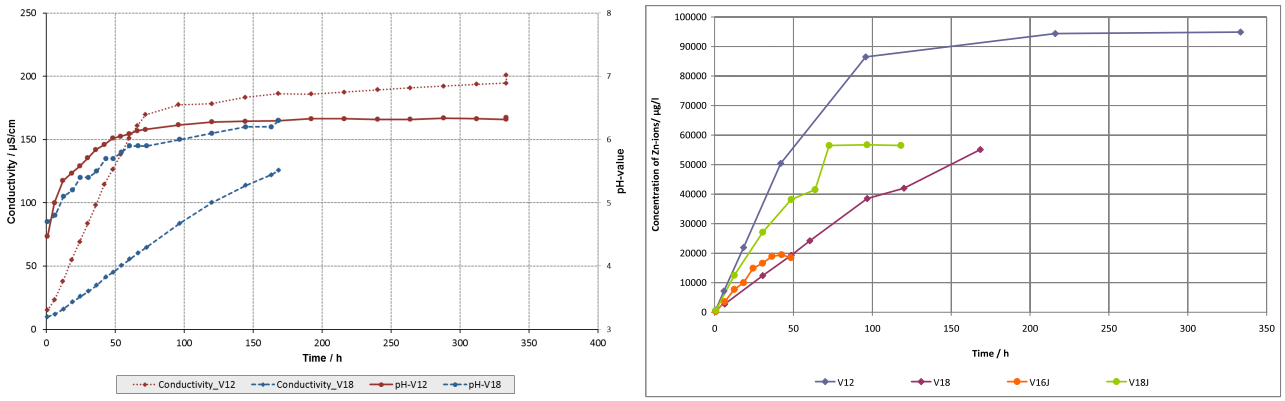

Figure 15: Dependencies of conductivity, pH-value and Zn-concentration during long-term corrosion experiments.

Condition	V12	V18	V16J	V18J
Lost mass of gratings	1600 g (total 3 units)	930 g	418 g	384.5 g (jet) 618.5 g (immersed)
Lost thickness (ρ_{Zn}=7.14 t/m³)	24 µm	42 µm	85 µm	78 µm (jet) 28 µm (immersed)
Theoretical concentration (lost mass/ fluid volume)	96.5 mg/l	56.1 mg/l	25.2 mg/l	60.5 mg/l
Chemical analyses (concentration of Zn-ions in the fluid)	94.9 mg/l ➔ equilibrium	55.1 mg/l ➔ no equilibrium	19.5 mg/l ➔ no equilibrium	56.7 mg/l ➔ no equilibrium

Table 2: Results of long-term corrosion experiments at ZSW.

Table 2 includes the lost masses of the gratings after the experimental runs. On the basis of these lost masses an average lost zinc thickness layer of the gratings and an average zinc concentration in the whole boric acid volume of the facility were calculated. The comparison of the calculated zinc concentrations caused by mass loss and the chemical analyses of the fluid shows good agreements for V12

and V18. Deviations were determined for the jet spray experiments V16J and V18J. The calculated average values give higher values to the chemical analyses for these two experiments. This effect can be explained by the corrosion progress at the jet spray gratings. In these experiments the pure zinc-layer (Figure 14) was removed and iron-rust particles were additionally released out of the hard-alloy-layer or the pure steel material. The maximum zinc-ion concentration at the equilibrium potential of a boric acid (13 g/l) at a temperature of T = 45 °C is about 90…95 mg/l. This zinc equilibrium potential was reached during V12 (Figure 15) and lead to a stagnation of zinc-ion release and the stabilization of the head loss (Figure 10). A zinc-ion release rate $R_{\text{Release}\,Zn}$ can be calculated on the basis of different measured parameters:

$$R_{\text{Release}\,Zn} = \frac{\Delta m(\Delta t)}{A_{\text{Corrosion}} \cdot \Delta t} = \frac{\Delta c_{\text{Zn}}(\Delta t) \cdot V_{\text{Fluid}}}{A_{\text{Corrosion}} \cdot \Delta t} = \frac{\rho_{\text{Zn}} \cdot \Delta s(\Delta t)}{\Delta t} \tag{1}$$

with: Δt - time difference, $A_{\text{Corrosion}}$ - corrosion surface, V_{Fluid} - fluid volume in the facility, ρ_{Zn} - zinc density, Δm - mass lost, Δc_{Zn} - concentration difference, Δs - abrasion thickness difference.

Figure 16 shows the dependencies of zinc-release rates on time and pH-value. The release rates are comparable for the experiments V12 and V18 during the first periods despite the different surface/volume-ratio of corrodible gratings to the same fluid volume. The release rates were constant up to a pH-value of about 6…6.1. A further increase of pH-value significantly decreased the release rate of immersed gratings. The release rate of a jet spray grating (V16J) in the first period of the experiment was significant higher as it was calculated for the immersed gratings. The release rate of V18J was calculated as an average value of the two installed gratings (spray jet, immersed) and shows a medium value.

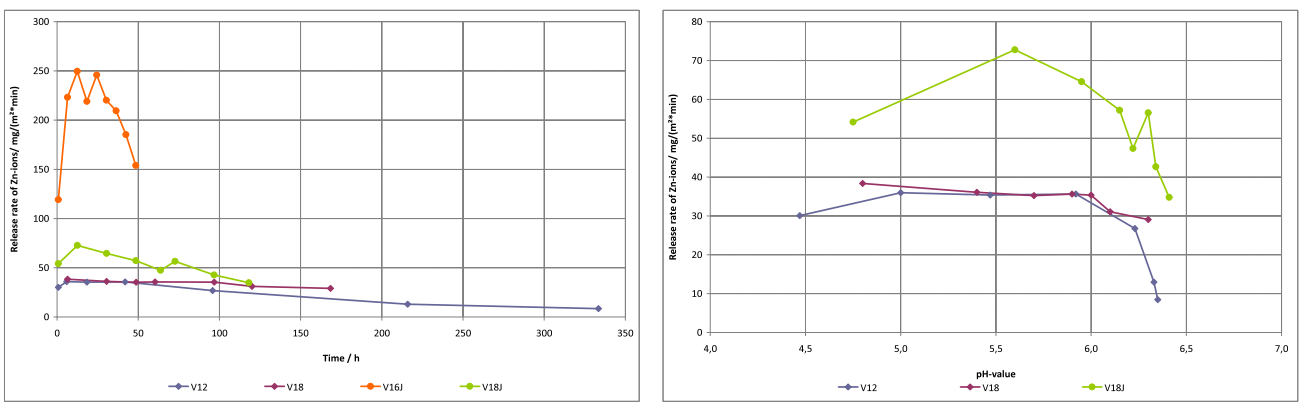

Figure 16: Dependencies of zinc-release rates on time (left) and pH-value (right).

Calculating an average abrasion thickness of all grating surfaces of (1) the discussed processes are well represented in Figure 17. The average abrasion thickness was stabilized at about 23 µm in V12. Local effects may produce iron rust particles. But, in average, the zinc layer of the gratings was not completely corroded (Figure 14). The absence of larger amounts of rust-particles also leads to a stabilization of the head loss. During the other experiments the average abrasion thickness reached the hard-alloy layer or the pure steel material with an adequate impact of iron-rust particles on the head losses.

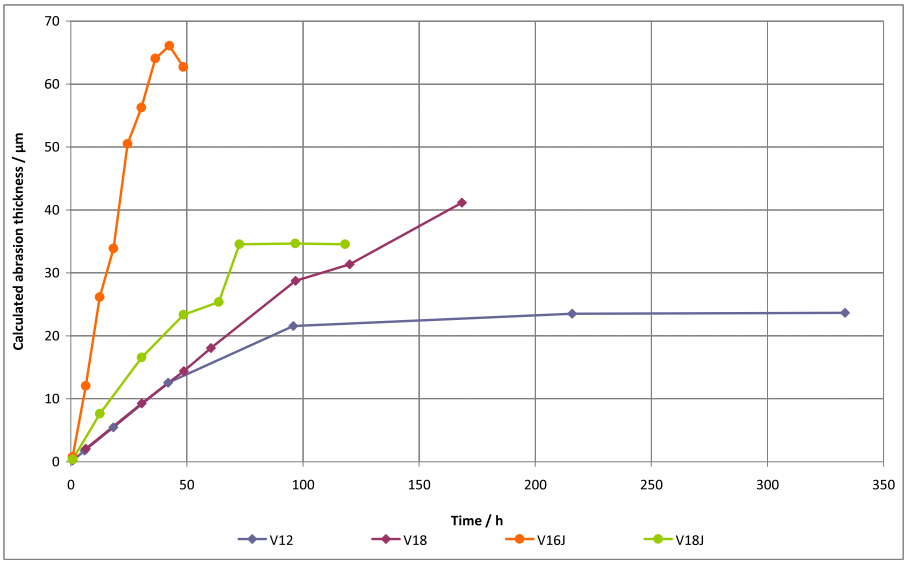

Figure 17: Calculated average abrasion thicknesses of the hot-dip galvanized gratings.

An average stability criterion was found for the corrosion progress on immersed gratings to define on which surface/volume ratios the head losses will be stabilized or not. The relation between necessary η-layer thickness of pure zinc and a necessary surface/volume ratio for a stabilization of the corrosion process is shown in Figure 18.

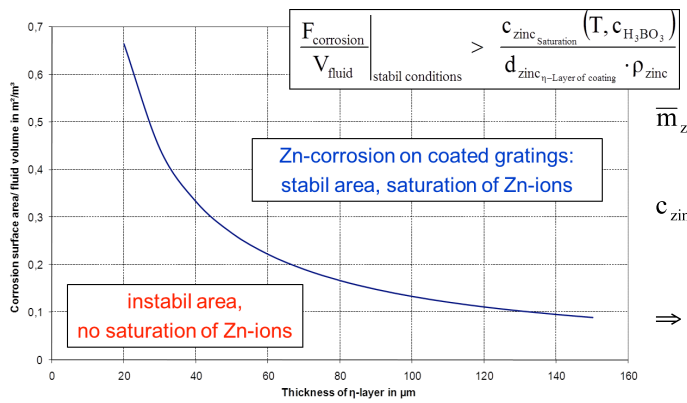

$$\left.\frac{F_{corrosion}}{V_{fluid}}\right|_{stabil\ conditions} > \frac{c_{zinc_{Saturation}}\left(T, c_{H_3BO_3}\right)}{d_{zinc_{\eta-Layer\ of\ coating}} \cdot \rho_{zinc}}$$

$$\overline{m}_{zinc_{solution\ at\ equilibrium}} < \overline{m}_{zinc_{\eta-Layer\ of\ coating}}$$

$$c_{zinc_{solution\ at\ equilibrium}}\left(T, c_{H_3BO_3}\right) V_{fluid} < d_{zinc_{\eta-Layer\ of\ coating}} \cdot F_{corrosion} \cdot \rho_{zinc}$$

$$\Rightarrow \left.\frac{F_{corrosion}}{V_{fluid}}\right|_{stabil\ conditions} > \frac{c_{zinc_{solution\ at\ equilibrium}}\left(T, c_{H_3BO_3}\right)}{d_{zinc_{\eta-Layer\ of\ coating}} \cdot \rho_{zinc}} \qquad (2)$$

Figure 18: Stabilization criterion for the influence of corrosion processes at immersed hot-dip galvanized gratings on the head loss increase in boric acid fluids at T = 45 °C.

5. Summary and outlook

Complex generic experiments were carried out to clarify phenomenological aspects and to generate parameters for CFD-modeling due to the LOCA-behaviour of insulation material in upwards and downwards components of a generic PWR sump considering long-term corrosion processes at hot dip galvanized steel gratings. The facility ZSW was designed to include the main components of an ECCS-flow path (sprayed leakage outflow, sump, pump, valves, FA-dummy) and to investigate the processes with generic flow conditions at generic scaled geometries. As a result of the experiments the phenomenology of the processes was determined. Flow-induced corrosion processes at hot-dip galvanized gratings depend on the material structure of the gratings, the water chemistry, the ratio between corrosion surface and fluid volume, the flow conditions and the momentum impact on the corrosion surfaces. Typical ambient conditions such as immersed gratings as well as gratings in air under a leakage spray jet

were considered. The influence of the corrosion processes on the head loss of mineral wool fibre filter cakes was estimated. Whereas the dissolution of zinc-ions as soluble corrosion products in boric acid does not influence the head loss in the filter cakes, the release of insoluble particulate corrosion products out of the hard-alloy layer or the pure steel leads to significant head loss increase up to the designed differential pressure of the sump strainers. The release of zinc-ions up to equilibrium potential into the boric acid reduces the corrosion process at immersed gratings as well as pH-values above 6.2. The possible stagnation of the corrosion process essentially depends on the surface/volume ratio. The spray jet induced corrosion showed the release of insoluble iron rust particles that rapidly increased the head loss at the filter cakes. Well filtering of corrosion products was observed in the sump strainer filter cake. The loss of the filter effect at the sump strainers by back flushing of the mineral wool fibre filter cakes caused the entry of corrosion products into the reactor core coupled with head loss increase at filter cakes in the FA-dummy. Systematic variations of fluid temperature, chemical conditions and the ratio between corrosion surface and fluid volume are planned for further experiments. The installation of a 2 x 2 mm meshed sump strainer and use of a 4 FA-dummy-cluster without bypass flow at the ZSW will improve the assignability to a generic German PWR.

6. Acknowledgments

The investigations described in this paper are funded by the German Federal Ministry of Economy and Technology under contract no. 150 1360 and 150 1363.

7. References

[1] Summary record of "Kick-off Meeting of the CSNI Task Group on Sump Clogging", OECD/NEA Headquarters, Issy-Les-Moulineaux, France, 2010, 23-24 November.

[2] W. Pointner, A. Bröcker: "The Barsebaek incident – generic aspects and international approaches", Proceedings Technical Meeting of the KTG: Current Topics of Reactor Safety Research in Germany, Dresden-Rossendorf, Germany, 2010, October 7-8.

[3] S. Alt, et al.: "Experiments for CFD-modelling of cooling water and insulation debris two-phase flow phenomena during loss of coolant accidents", CD-proceedings paper 22, NURETH-12, Pittsburgh, Pennsylvania, U.S.A., 2007, September 30-October 4.

[4] S. Alt, R. Hampel, W. Kästner, F. Zacharias: "Experimente zum integralen Verhalten von isolationsmaterial-belasteten Kühlmittelströmungen", Proceedings Jahrestagung Kerntechnik 2010 paper 220, Berlin, Germany, 2010, Mai 4-6.

[5] U. Waas: "Untersuchungen zu DWR: Freisetzung des Isoliermaterials, Transport zum Sumpf, Verhalten im Sumpf, Siebbelegung und Langzeiteffekte", CD-ROM Proceedings KTG-Fachtag, Rossendorf, Germany, 2006, April 3-4.

[6] E. Krepper, et al.: "Numerical and experimental investigations for insulation particle transport phenomena in water flow", Annals of Nuclear Energy 35 (2008), pp. 1564–1579.

[7] E. Krepper, et al.: "CFD analyses of fibre transport and fibre deposition at plunging jet conditions", Proceedings Technical Meeting of the KTG: Current Topics of Reactor Safety Research in Germany, Dresden-Rossendorf, Germany, 2010, October 7-8.

[8] H. Kryk, W. Hoffmann, U. Waas: "Influence of Corrosion Processes on the Head Loss across Sump Strainers", Proceedings Technical Meeting of the KTG: Current Topics of Reactor Safety Research in Germany, Dresden-Rossendorf, Germany, 2010, October 7-8.

[9] S. Alt, et al.: "Generic experiments at the sump model "Zittauer Strömungswanne" (ZSW) for the behaviour of mineral wool in the sump and the reactor core", Kerntechnik, Vol. 76, 2011, pp. 20-29